


ORIGINAL RESEARCH

In search of the glow—Three-dimensional reconstruction of *Latia neritoides* with specific focus on the mantle cavity (Mollusca; Gastropoda; Hygrophila)

S. Greistorfer¹, I. Miller² , J. von Byern¹, V. B. Meyer-Rochow^{3,4}, S. H. Geyer⁵, W. J. Weninger⁵ & G. Steiner¹

¹Unit for Integrative Zoology, Department of Evolutionary Biology, University of Vienna, Vienna, Austria

²Institute of Medical Biochemistry, University of Veterinary Medicine Vienna, Vienna, Austria

³Department of Ecology and Genetics, Oulu University, Oulu, Finland

⁴Agricultural Science and Technology Research Institute, Andong National University, Andong, Korea

⁵Division of Anatomy, Center for Anatomy and Cell Biology, Medical Imaging Cluster, Medical University of Vienna, Vienna, Austria

Keywords

medical applications; gland cells; ultrastructure; bioluminescent; defence system; snails; *Latia neritoides*; 3D model.

Correspondence

Ingrid Miller, Institute of Medical Biochemistry, University of Veterinary Medicine Vienna, Austria.

Email: ingrid.miller@vetmeduni.ac.at

Sophie Greistorfer, Unit for Integrative Zoology, Department of Evolutionary Biology, University of Vienna, Austria.

Email: sophie.greistorfer@univie.ac.at

Editor: Gabriele Uhl

Received 13 May 2023; revised 18 February 2024; accepted 20 February 2024

doi:10.1111/jzo.13161

Introduction

The exceptional location of New Zealand as a group of fairly isolated islands has made the country a perfect place to study animals that had evolved in relative solitude over a long period. Certain freshwater streams and some lakes of New Zealand's North Island are the home of *Latia neritoides*, an endemic and unique gastropod (Meyer-Rochow & Moore, 1988). Originally described by Grey (1850), scientists started more than 100 years ago to study the behaviour of this fascinating bioluminescent species (Hutton, 1881; Pelse-ner, 1901; Ponder, 1964; Suter, 1913). Tissue examinations of the animal as well as dissections led to descriptions of its morphology and anatomy (Eales, 1923; Hubendick, 1945; Pelse-ner, 1901). Later a comparative study of the various members

Abstract

The freshwater snail *Latia neritoides* occurs in certain streams and lakes of New Zealand's North Island. It defends itself against predators with a unique mechanism – the release of sticky, glowing mucus. Two possible origins of this defence mucus had earlier been suggested: the foot and the pneumostome area. After examining the glandular system of the foot in a previous study, in the present study we examined the general morphology of *L. neritoides*, focusing on the mantle cavity. With the first complete 3D model of *L. neritoides* now available, it is possible to evaluate previous morphological studies and to give non-specialists a better understanding of the soft part anatomy of this fascinating gastropod. As a by-product of this, we also compared the capabilities of μ -CT and HREM on a methodological level. We characterized the two most common gland types in the mantle cavity (Lmcg1/Lmcg2) on the basis of their ultrastructure. They are present in large numbers and, therefore, regarded as likely candidates for being the producers of one or more components of the defence mucus. This notion was confirmed by histochemical analyses of Lmcg1 and Lmcg2 and other gland types in *L. neritoides*.

of the group, formerly known as Basommatophora and then including *L. neritoides*, was published (Hubendick, 1978). The central nervous system of *L. neritoides* was compared with that of related Pulmonata by Haszprunar and Huber (1990) and the latest comprehensive pieces of research on the ecology, general biology and morphology of *L. neritoides* were those of Meyer-Rochow and Moore (1988), and Moore and Meyer-Rochow (1988). A book chapter summarized different aspects of *L. neritoides*' internal anatomy (Meyer-Rochow & Moore, 2009) and an ultrastructural study by Meyer-Rochow and Bobkova (2001) provided a comparison of the eyes of the luminescent *Latia neritoides* with those of a non-luminescent snail species of the genus *Ancylus*.

Latia neritoides belongs to the Hygrophila, whose molecular phylogeny has only recently been a subject of study by Saadi

et al. (2020). The first impression of this animal is relatively unspectacular. It has a limpet-like shell commonly measuring 8.5–10 mm in length, which is of brownish coloration and provides an excellent camouflage on the stones that *L. neritoides* individuals are attached to while feeding on diatoms (Bowden, 1950; Hubendick, 1945; Meyer-Rochow & Moore, 1988). In addition to camouflage, a variety of defence mechanisms have evolved among freshwater gastropods, ranging from an active use of their own shells as a weapon (Mori et al., 2016) or a sealed panic room (Kelly & Cory, 1987) to the production of a defence mucus (Gould et al., 2019; Mair & Port, 2002; Martin & Deyrup-Olsen, 1986). In *L. neritoides* the latter is bioluminescent and sticky.

Bioluminescence employed for hunting, communication or as a form of defence (Haddock et al., 2010; Widder, 2010) is well known in marine animals, but uncommon for gastropods. While only a few species of gastropods are capable of emitting light at all (Counsilman et al., 1987; Counsilman & Ong, 1988; Deheyn & Wilson, 2011; Marshall, 1997; Oba & Schultz, 2014; Ponder, 1988), *L. neritoides* is still the only bioluminescent freshwater snail. When under pressure from a predator such as *Archichauliodes diversus* (Insecta, Megaloptera) and dragonfly larvae or fish, *L. neritoides* ejects a greenish glowing, sticky mucus (Meyer-Rochow & Moore, 1988). This mucus' properties not only startle the attacker; owing to its stickiness, the mucus clings to the attacker and *L. neritoides* has time to escape. Moreover, glowing mucus droplets being carried downstream by the current distract the attackers and cause them to chase the droplets, rather than to locate the producer of the droplets (Meyer-Rochow & Moore, 1988). Another function of this mucus is that when used at night or in some darker under water areas, it may temporarily blur the sight of the hunter. As the living environment of *L. neritoides* are mainly freshwater streams, the glowing mucus gets distributed over a wide area in a short time, especially when produced by more than one animal, thereby obscuring the exact location of the snail.

The closest relatives of *L. neritoides* belong to the South American family Chiliniidae (Ovando & Gregoric, 2012; Saadi et al., 2020). The question, therefore, arises what makes this species so different and why only *L. neritoides* and none of the other freshwater gastropods have evolved bioluminescence for defence.

While some studies on the chemical components of the mucus exist (Ohmiya et al., 2005; Shimomura et al., 1972; Shimomura & Johnson, 1968a, 1968b), less research has focused on the underlying glandular system (Bowden, 1950; Meyer-Rochow & Moore, 1988). Earlier studies suggested two different production sites for *L. neritoides*' defence mucus (Bowden, 1950; Meyer-Rochow & Moore, 1988). The lateral area/furrows of the foot, with two gland cell types held accountable for the mucus, were already investigated by various methods (Bowden, 1950; Greistorfer et al., 2023a, 2023b). We cannot exclude that these gland cell types in the lateral area of the foot (named L11/L21) are indeed part of the defence system, but more likely they secrete just one component (Greistorfer et al., 2023a). After all, the mucus is not just sticky, but luminescent as well. Therefore, it presumably

contains a combination of several components which derive from different parts of the body.

Another candidate for the origin of defence mucus components is the mantle cavity, as the glowing substance appears around or at the pneumostome (Greistorfer et al., 2023a; Meyer-Rochow & Moore, 1988). Before concentrating on the mantle cavity, we set it in an anatomical context by means of a 3D reconstruction of the whole animal, allowing to compare the results of these modern high-resolution methods with those of previous publications (Eales, 1923; Hubendick, 1945; Meyer-Rochow & Moore, 2009; Pelseener, 1901). We had a detailed look at the mantle cavity and the pneumostome area. They contain gland cell types that were examined histologically in order to evaluate the possibility that they are the origin of the glowing component.

Materials and methods

Specimen collection

Adult individuals of *Latia neritoides* were collected during a sampling trip in January 2019 on the North Island of New Zealand (river near Kawhia, S38°05'40.8" E175°06'31.3"; Mangawhitikau river, S38°14'16.5" E175°01'20.8") and identified by DNA barcoding. Animals were fixated directly after sampling (see Greistorfer et al., 2023a).

Investigation of the shell surface vegetation and the radula

The shell was air-dried after the fixation in 96% EtOH. The soft parts were fixed in 96% EtOH, too. At the University of Vienna, Austria, the animal was transferred to 100% acetone, frozen in liquid nitrogen, fractured and transferred back to 100% acetone. The samples were dried in the critical point drier Leica EM CPD300. They were mounted with a double carbon foil on aluminium stubs, stabilized with silver and coated for 120 s with a gold layer (sputter coater: JEOL JFC-2300HR). The observations were made using a scanning electron microscope (JEOL IT 300 LaB6 LV, Jeol Germany GmbH) at 20 kV.

Diatom identifications are based on the identification tool <https://www.landcareresearch.co.nz/> (used on 10.12.2022) and the Quick Guide to Common Diatom Genera in Freshwaters (Kilroy, 2020).

Gland morphology

Sectioned parts of a specimen were fixated in 2.5% glutaraldehyde buffered with sodium cacodylate (0.1 M, pH 7.4, plus 10% sucrose) for 2 h. The material was further processed and embedded as described in Greistorfer et al. (2020). Afterwards the material was cut into 70 nm thick sections with an ultra-diamond knife (Co. Diatome AG, Switzerland) at a Leica UC6 ultramicrotome (Co. Leica Microsystems GmbH, Wetzlar, Germany), mounted on copper grids and stained with uranyl acetate. Observations were made with a Zeiss Libra 120 transmission electron microscope (Co. Carl Zeiss AG, Germany)

operated at 120 kV. Measurements were taken on ultrastructural images and represent mean values of 10 measurements.

Gland histochemistry

For histochemical analyses of the gland cell types, six animals, fixated in Carnoy's solution (Aesch et al., 2010) for 3 h at room temperature, were embedded and serially sectioned (7 μ m). Four of them were transversely sectioned, two from dorsal to ventral, while two animals are horizontally sectioned. For serial sectioning the animals were cleared in methyl benzoate, infiltrated with a benzene – paraffin mixture (50%/50%), followed by 100% paraffin (Merck, Germany) overnight. The 7 μ m sections were cut with a rotary microtome (Leica RM2265, Co. Leica Biosystems GmbH, Germany), transferred to standard object slides using Ruyter's solution (Ruyter, 1931) and dried overnight at 35°C in a heat cabinet (Binder GmbH, Germany).

Histochemical stainings used are periodic acid Schiff (PAS) staining, including negative control with acetylation (McManus & Mowry, 1960), for the detection of hexose containing mucosubstances, Alcian blue G8X staining (McManus & Mowry, 1960) at pH 1.0 and 2.5 and Toluidine blue O (Mulisch & Welsch, 2010) at pH 4.3 to detect sulphated and carboxylated acidic mucosubstances, Biebrich scarlet staining (pH 6, 8, 9.5 and 10.5) (McManus & Mowry, 1960; Spicer & Lillie, 1961) for visualizing basic proteins. Also a combination staining of PAS and Alcian blue was done. Furthermore, von Kossa (Sheehan & Hrapchack, 1980) and Alizarin red S (Aesch et al., 2010) stainings were used for calcium detection, and for the documentation of L-3,4-dihydroxyphenylalanine (L-DOPA), Arnow staining (Arnow, 1937) was applied. Alcian blue staining (pH 1) was combined with Azan trichrome staining (Heidenhain, 1905) for a better visualization of the gland cells in contrast to the surrounding tissue. All object slides were sealed with cover slips using the mounting medium DPX new (Merck, Germany).

Graphical representation and 3D reconstruction

For assessment of internal anatomy of *L. neritoides* 3 different specimens were used.

All specimens were fixed and stored in Bouin's solution (Aesch et al., 2010). After rinsing them for 1 h, they were dehydrated in a series of ethanol (50% 1 h, 70%, 80%, 90%, 100% 4–5 h each). They were stored in 100% ethanol, before further processing.

Each specimen was examined with a different method (μ -CT, HREM, serial sections). The complete 3D model of *L. neritoides* is based on a μ -CT data set. For this scan one animal was stained for 24 h in a 1% alcoholic iodine solution (Carl Roth GmbH 1 Co. KG, Karlsruhe, Germany; cat. #X864.1). Four washing steps were done in 99.8% ethanol, then the snail was placed in a plastic tube and scanned in 99.8% EtOH with an Xradia XCT (Zeiss, Germany). The scanning parameters were 60 kV, 83 μ A and 20 s exposure time resulting in a pixel size of 2.67 μ m. The data were converted

to a conventional format using the Fiji plugin XRM reader (Metscher, 2022).

The nervous system was reconstructed based on an HREM (high-resolution episcopy microscopy; voxel size 2.63 μ m) and a second image stack, which was based on 7 μ m serial sections. The sample was processed for HREM following standard protocols (Geyer et al., 2017; Mohun & Weninger, 2012a, 2012b). It was infiltrated with and embedded in methacrylic resin (JB-4, Polysciences, Warrington, PA, USA) containing 0.4 g eosin per 100 mL. The resin-block was sealed to allow for polymerization under oxygen-free conditions at room temperature for 24 h and then baked at 90°C for 48 h. The HREM data were generated with an Optical-HREM apparatus (Indigo Scientific Ltd., Baldock, UK) with a section thickness of 2.63 μ m.

7 μ m serial sections of another specimen were prepared as described in gland histochemistry and stained with HE (Haematoxylin-Eosin-staining; Aesch et al., 2010). Images of whole specimens and serial sections were taken with a Nikon SMZ 25 (Nikon, Tokyo, Japan). For detailed visualization, a Nikon Ni-U compound microscope with a mounted Nikon Ds-Ri2 camera was used.

All image stacks (HREM, μ -CT, serial section) were reconstructed by labelling using the segmentation editor of Amira software (version 6.4, FEI Company). The label files of some materials, together with the μ -CT data set, were uploaded to Biomedisa (Lösel et al., 2020) and resegmented for refinement. The section series was aligned with the 'align slices'—tool in Amira before the labelling. The surfaces were generated in Amira with the 'generate surface'—tool. The triangulation was then reduced by the simplification editor and the surface was smoothed using the 'smooth surface'—tool. The finalized surfaces were exported as a wavefront (*.obj) file. For final visualization the surfaces were imported into the software Blender (v. 3.2.0, GNU General Public Licence). Each material was customized with unique colours using the Principled BSDF node in the Shader Editor. To achieve transparency effects, the Glass BSDF, Transparent BSDF and Mix Shader nodes were used. All images were further processed with Photoshop CS6 (Adobe Systems, San Jose) for background and brightness adjustments. Photoshop was also applied for assembling of figures (e.g. labelling of structures).

For the animations, which were done in Blender, various light objects like Sun or Spotlights were included to enhance the background. In specific scenes, the HDRI 'Blue Grotto' by Greg Zaal, available under the CC0 licence from Poly Haven (<https://polyhaven.com/>), was utilized to achieve more realistic lighting effects. The animations for the scenes were meticulously crafted by inserting keyframes in the Dope Sheet by utilizing the Timeline. This approach was used both to animate the camera and to make the scene more lively.

To animate the mucus, Blender's internal fluid simulation, located within the physics tab, was used. It is important to note that the shell and gland cells, along with their contents, were the only components newly created in Blender. The foundational structure was crafted in edit mode, refined later in sculpt mode. To create the appearance of moss, particle settings were employed.

All images were rendered using the Cycles renderer, exported as TIFF files, and subsequently assembled into an animation within the Blender video editor. Images integrated into the video were added either directly in Blender using the 'Images as Planes' add-on or during the video editing process in Adobe Premiere Pro Version 23.2.0 (Build 69, Adobe Systems, San Jose). The post-processing, editing and labelling of the animations (Videos S1 and S2) were done using Adobe Premiere Pro CS5 (Adobe Systems, San Jose).

Terminology

According to the nomenclature of Smith (2006) the identified gland cell types were addressed as follows: the first letter referring to the animal, in this case 'L', followed by the location and an identification number.

Results

External morphology

Latia neritoides resembles a limpet (Fig. 1). In ventral or lateral view, *L. neritoides*' strong muscular foot with the pneumostome lappet comes into sight (Fig. 1a,c). Two roundish tentacles with eyes at their base are visible (Fig. 1a). *L. neritoides*' brown shell covers the whole body and in older individuals is overgrown by diatoms (Bacillariophyceae) and other unidentified life epiphytes (Figs 1e and 2a–e). The overgrowth was tentatively identified as *Cocconeis splacentula* (Fig. 2a–d, blue), with pinnate diatoms also present (Fig. 2a,b,d, green). *Rhoicosphenia* sp., *Gomphonema* sp., *Cymbella* sp. or *Encyonema* sp. might have been present, but a clear statement cannot be given as raphe and frustule patterns were not clearly visible. The brown-coloured as well as the yellow material cannot be identified, but in all likelihood consists of algae and spores (Fig. 2a–e). *L. neritoides*' blade-like teeth are shown in scanning electron images (Fig. 2f,g). On the right side of the shell a calcified ridge and an elongated extension on the inner side of the shell are noticeable (Fig. 1f, white square).

Morphology of the glands identified in the mantle cavity

One of the main objectives of this study is the characterization of the gland cell types in the mantle cavity and the pneumostome area (Fig. 1a–c, asterisks), where the glow of the defence mucus first appears (Fig. 1d, dotted square; Video S1). In this area a pneumostomal lappet is present (Figs 1a and 3a,b; Video S1). The pneumostome becomes clearly visible in the reconstruction of *L. neritoides* (Fig. 3a–c, dotted square). The reconstruction of the mantle cavity (Fig. 3c,d; Video S1) locates its opening, the pneumostome (highlighted in green in Fig. 3b), at its right posterior end. In the vicinity of the pneumostome outside the mantle cavity are two large clusters of pedal gland cells, L11/L21 type glands (Fig. 3c,d). These cell types are distributed on lateral foot area, on the mantle and the oral lappet; in this study only a part of them is reconstructed

to show the positional relationship. The mantle cavity itself is filled with mucus, especially in the anterior region (Fig. 4a, dotted red line).

The whole mantle cavity is a highly active area covered with microvilli and, in some parts, cilia (Fig. 4b–g). At ultra-structural level, two common gland cell types, present in large numbers, were identifiable (Fig. 4b–g; Video S1). Both were epithelial (Fig. 4a,g) and present in the mantle cavity's anterior (Fig. 4a–f) as well as situated in the middle part of the animal (Fig. 4g,h). The first gland type (Lmcg1) has globular vesicles that burst open, when the granular content is released (Fig. 4b,c,g). With diameters of 2.5 µm the vesicles are crammed inside the gland cells. In this gland type also rough endoplasmic reticulum is prominent, mostly at the lower end of the cell, but also between the vesicles, it is detectable (Fig. 5a).

Next to the Lmcg1, gland type Lmcg2 is located (Fig. 4g). This gland type is shown in different stages (Figs 4d,e,g and 5c). Many mitochondria are present, but also the amount of present Golgi seems to be higher than in Lmcg1 (Fig. 5b), where Golgi are detected too (Fig. 5d). Both gland cell types are around 7 µm in length. It was not possible to determine if a third gland cell type was present or if the detected gland cell represented a stage of Lmcg1 (Fig. 4f). Nevertheless, the releasing mechanism of the granular content seemed to be different. Underneath the glands, in the posterior part of the mantle cavity (Fig. 4g–i) a kind of storage supplied with muscle fibres is present (Fig. 4i). No duct or other connection to the mantle cavity was observed. Also directly underneath the gland area muscles are visible (Fig. 5e).

Gland histochemistry

Lmcg1 shows a strong reaction to some histochemical stains, while Lmcg2 does not react at all (Fig. 6a, black square, e, h; Table 1; Video S2). A strong reaction to PAS as well as Alcian blue (both pH levels) is shown in this gland type indicating the presence of sulphated and carboxylated glycoproteins.

The salivary gland shows a similar reaction, but an additional positive reaction to the toluidine blue stain, even if weak, proves that in this gland, too, acidic proteins are present (Fig. 6a; Table 1; Video S1). Not all gland cells show the same reactivity: some react only positive for proteins, others only for carbohydrates (Fig. 6b; Video S2). Another interesting finding is that gland cell types in the spermoviduct (Lsog1) alone give a positive reaction to basic proteins (Biebrich Scarlet staining pH 6, 8.5, 10.5) (Fig. 6d; Table 1; Video S2). In Lsog2, present in another section of the spermoviduct, sulphated and carboxylated glycoproteins are detected (Fig. 6c, d; Table 1; Video S2). Here too, the only strong reaction to acidic proteins in the animal is present (Toluidine blue staining, pH 4.5) (Table 1). Sulphated and carboxylated glycoproteins are also detected in the albumen gland, a gland cell type in the penis area (Lpag) and the midgut gland, although the reaction in the midgut gland was very weak (Fig. 6f,g,j; Table 1; Video S2).

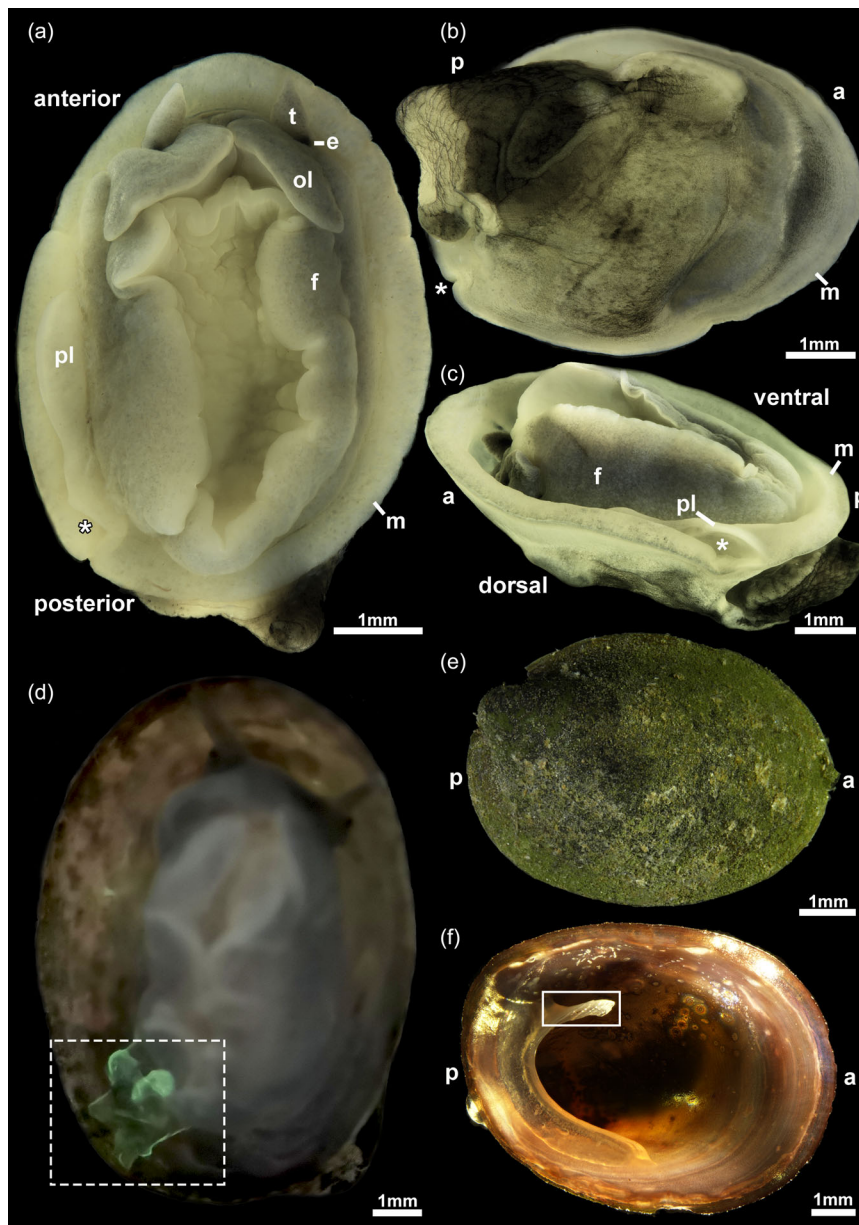


Figure 1 Habitus of *Latia neritoides*. (a) Ventral view. Head with non-retractable tentacles and oral lobes is visible. The pneumostome area, where defence mucus is released, is marked with an asterisk. (b) Dorsal view. The shell is dissolved, so an unrestricted access of the mantle, covering the inner organs, becomes possible. The area of defence release is marked with an asterisk. (c) Lateral view. This view allows an insight to the pneumostome area. (a–c) The animal is fixed with Bouin solution. (d) Dorsal view of a living animal while releasing the defence mucus, marked with a dashed square. (e) Dorsal view on a shell. Most of the shells of older individuals are inhabited by other living organisms like algae and diatoms. (f) Ventral view of a shell. The projection of the shell (square) is clearly visible. a = anterior, e = eye, f = foot, m = mantle, ol = oral lobe, p = posterior, pl = pneumostomal lobe, t = tentacle.

Close inspection of the gut loop of *L. neritoides* identified two different gland cell types: Lgg1, showing a positive reaction to PAS, Alcian blue (both pH levels) and weak reaction with Toluidine blue (pH 4.5) and an Lgg2, which does not react to any stain (Fig. 6i,k; Table 1; Video S2).

Morphology of the digestive tract

Latia neritoides' prominent oesophagus, reaching to the middle of the animal, is guarded on the left and right by the salivary gland (Figs 7a,b,d and 8; Video S2). The gland reaches from the beginning of the radula sack, at the anterior end of the

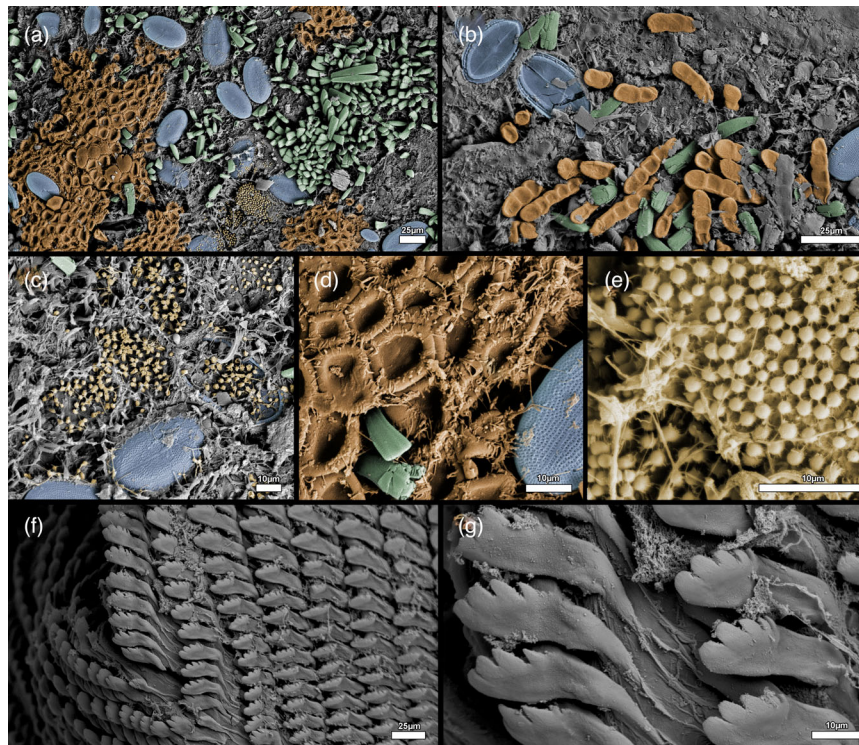


Figure 2 Scanning electron analyses of the shell surface vegetation (with false coloration) and the radula of *Latia neritoides*. (a–d) *Cocconeis placentula* coloured in blue. (a, b, d) *Pennate diatoms* coloured in green. (a) View on a broad area of the shell with different diatoms visible. (b) *Cocconeis placentula* und *pennate diatoms* next to each other. (c) Places where *Cocconeis* died are populated by algae. (d) A close up on *Cocconeis* and one of the pennate diatoms next to algae and maybe spores. (e) A close up on algae/spores. (f, g) Detailed view on the radula teeth.

oesophagus, to nearly the end of it (Fig. 8b,e; Video S2). Just underneath the oesophagus the radula with the odontophores is situated (Figs 7a,b,d and 8b–f; Video S2). The radula's teeth are shovel-like, curved and toothed at their edges (Fig. 2f,g; Video S2). The radula's musculature covers the radula sack and the odontophores (Figs 7 and 8d–f; Video S2). The radula complex occupies considerable space in the anterior part of *L. neritoides*. Following the oesophagus further into the animal, a gizzard with a caecum becomes visible (Fig. 8; Video S2). Only one intestinal loop, embedded in the midgut gland, is present (Figs 7 and 8; Video S2). Both are situated above the other organs (Fig. 7a,d; Video S2). The anus ends in the mantle cavity, near the pneumostome area (Figs 7a and 8a,d; Video S2).

Morphology of the nervous system

We have reconstructed the nervous system of three specimens, using a different method in each case (μ -CT, HREM, serial sections) (Fig. 9). On the ventral side of the animal, two prominent pedal ganglia are connected with a broad commissure and an additional, slender parapedal commissure (Fig. 9a–d,g,h). The foot is innervated by two bifurcating nerves originating from the ventral side of these pedal ganglia (Fig. 9e–h). Laterally, two connectives project from each pedal ganglion. On each side, one connective extends dorsolateral to the pleural

ganglion that is followed by the parietal ganglion. More anteriorly, the second connective connects to the cerebral ganglion (Fig. 9c–h).

The cerebral ganglia are connected by a broad cerebral commissure and give off two nerves to the anterior part of the animal (Fig. 9c–f). Anteromedially of the cerebral ganglia two buccal ganglia, connected by a commissure, are present (Fig. 9d,f,h). The cerebro-buccal connective is thin and barely visible (Fig. 9b,d,f). The nervous system of *L. neritoides* is asymmetric. The parietal ganglia are located close to the pleural ganglia, with the distance being larger on the right side (Fig. 9c,d,g,h). The supraoesophageal ganglion on the right side innervates the osphradium. The visceral loop is completed by the closely adjacent visceral and suboesophageal ganglia (Fig. 9c,d,g,h).

Morphology of the reproductive system

The most prominent reproductive organs in *L. neritoides* are the ovotestis, spermoviduct and albumen gland. The ovotestis is located at the animal's posterior end, together with the midgut gland filling the apex region (Fig. 7; Video S2). In dorsal view the albumen gland covers the spermoviduct and borders the intestinal loop (Figs 7a,c and 10a,c,d; Video S2). The spermoviduct is passing over the uterus (the outer border is not reconstructed), followed by the vagina (Figs 7b and 10b,c;

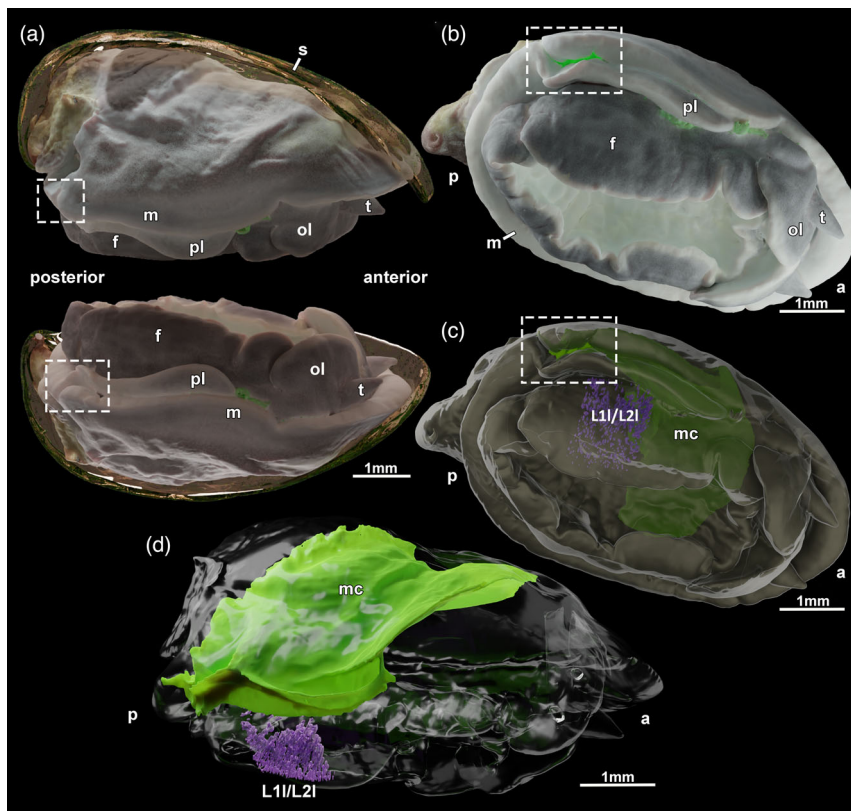


Figure 3 Reconstruction of *Latia neritoides* with localization of the pneumostome area. (a) Display with only half of the shell shown, so the pneumostome area becomes visible. (b) Ventral view. Release of the defence mucus shown in glowing green. (c, d) The mantle cavity is shown in green. The gland types L1I & L2I (Greistorfer *et al.*, 2023a) are situated all over the *L. neritoides*' foot. Here they are only partly reconstructed. (a–c) Pneumostome area is marked with a dashed square. a = anterior, f = foot, m = mantel, mc = mantel cavity, ol = oral lobe, p = posterior, pl = pneumostomal lobe, s = shell, t = tentacle.

Video S2). The latter has its opening near the anterior border of the pneumostome opening (Fig 7b; Video S2). The vas deferens connects the spermoviduct to the penile apparatus (pa) (Figs 7 and 10; Video S2). The opening of the male reproductive organ is near the base of the right tentacle (Figs 7a and 10a; Video S2). Connected to the uterus is the duct of the spermatheca, which is situated on the left side of the body (Figs 7b and 10a,b,d; Video S2).

Morphology of the heart and kidney

The dorsal view of *L. neritoides* shows on the left the closed pericardium with two atria (Fig. 7a,b,d) and on the right the kidney (Fig. 7a–d), which opens into the mantle cavity and is directly attached to the heart.

Discussion

General aspects

The external appearance of *Latia neritoides* has already been described repeatedly (Eales, 1923; Grey, 1850; Hutton, 1881; Meyer-Rochow & Moore, 1988; Moore & Meyer-

Rochow, 1988; Pelseneer, 1901; Ponder, 1964; Suter, 1913). Observations on well-preserved specimens in previous investigations (see citations above), are congruent with this study's results. *L. neritoides* has a limpet-like shell, a strong muscular foot and round unretractable tentacles with eyes at their bases. The retractor muscle for the tentacle, featured in earlier investigations (Hubendick, 1945), is missing. The dark greyish pigmented skin on the upper side of the animal may be interpreted as a camouflage on the stones, even if the foot of the animal seldom can be seen projecting out from the shell (Eales, 1923; Ponder, 1964). The shape of the shell as an adaption to its surroundings, the freshwater streams, has already been commented on by Meyer-Rochow and Moore (1988). The strong foot is vital to survive in the streams as the animals have to cling to the rocks they are grazing on. Movement is based on cilia, but the suction cup effect of the muscular network is not to be underestimated (Moore & Meyer-Rochow, 1988).

Scanning electron images revealed different diatoms present on the shell of *L. neritoides*. It is known that the animals are feeding on them, because *Cocconeis sp.*, *Epithemia sp.*, *Achanthes sp.* and *Stauroneis sp.* (all Bacillariophyceae) were found in the stomach (Bowden, 1950; Meyer-Rochow &

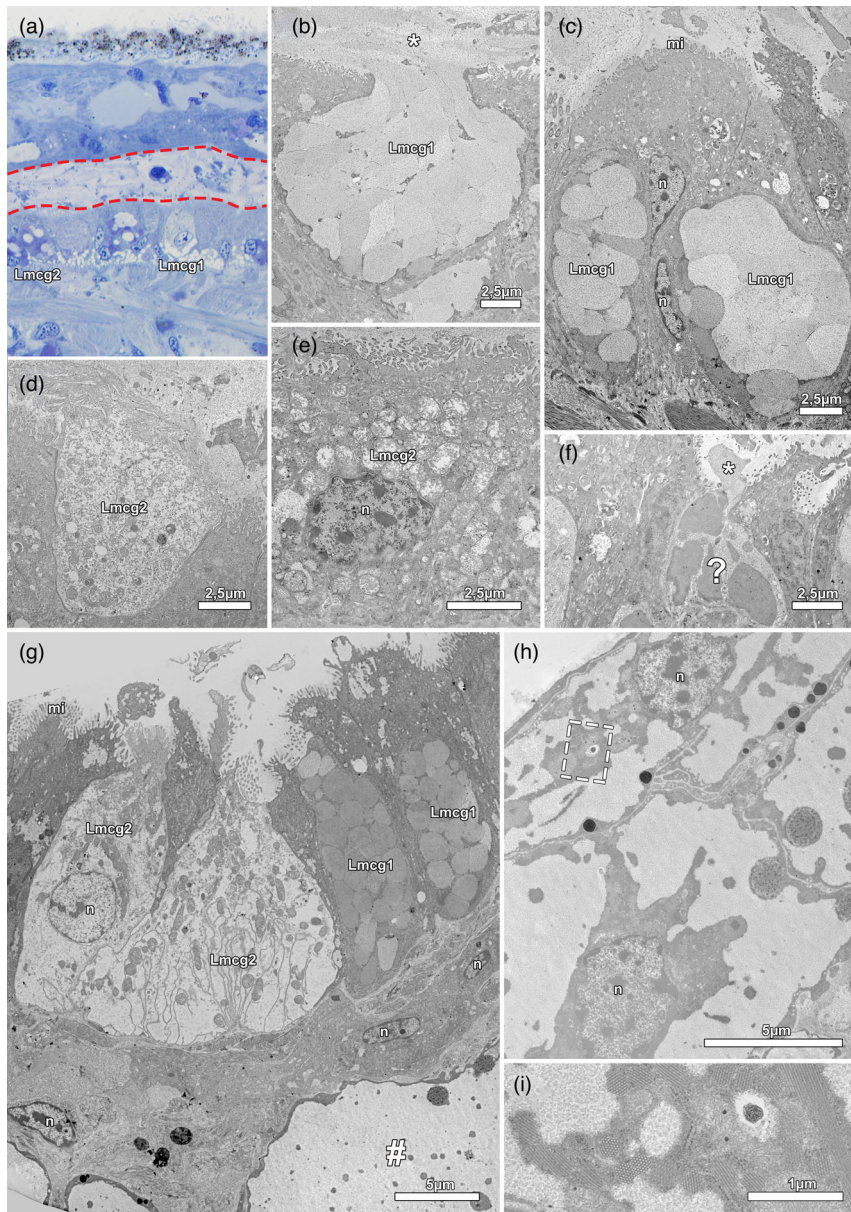


Figure 4 Ultrastructure of the mantle cavity of *Latia neritoides*. (a) Semithin section providing an overview of the area shown in the TEM images. The mantle cavity is marked with the red line. Images (a–f) show investigations from the anterior part, while (g–i) show images from the middle part. (b) The granular content of gland cell type Lmcg1 (*Latia* mantle cavity gland 1) shows densely packed vesicles, which disrupt when released (asterisk). (c) In the image two gland cells of Lmcg1 are shown next to each other with a very compressed nucleus (n). (d, e) Different to the gland cell type Lmcg1, gland cell type Lmcg2 is a holocrine gland cell type. In image (d) it is shown in a later stadium without a nucleus, in image (e) it is shown with the nucleus. (f) A gland cell type, marked with ?, for which it is unknown if it is a different stage of Lmcg1 or third gland type. The release of the cell content is shown and marked by an asterisk. (g) Direct comparison between the gland cell types Lmcg1 and Lmcg2, situated in the epithelium. A # marks an area situated next to the gland cells, pervaded with myosin filaments. (h) The area # in more detail. A square marks the area in picture i. (i) Detailed view on some of the presumptive myosin filaments. mi = microvilli, n = nucleus.

Moore, 1988). The scanning electron images show cup-shaped teeth with 5 elongations, ideal for scraping off diatoms from stones, even if some of the teeth may be malformed or damaged from excessive use (Meyer-Rochow & Moore, 2009).

For the elongated extension on the inner side of the shell, it is assumed, that it is used to hold the pneumostome open (Bowden, 1950; Meyer-Rochow & Moore, 1988), while the lamella as well as the extension serve as important fixation points for the shell (Bowden, 1950).

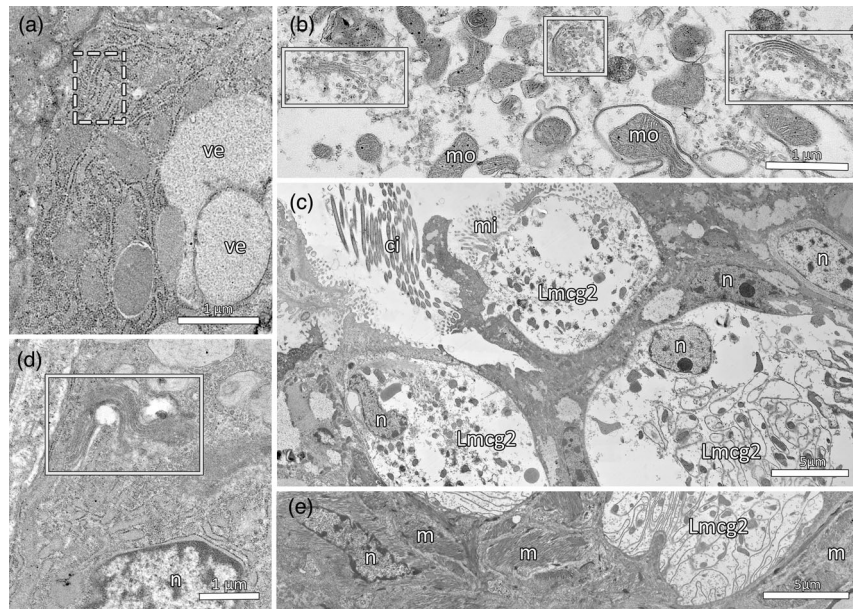


Figure 5 Ultrastructure of the gland cell types Lmcg1 and Lmcg2. (a) Rough endoplasmic reticulum (dashed square) is detectable next to the vesicles of gland cell type Lmcg1. (b) A large number of Golgi (square) and mitochondria are found in the gland cell type Lmcg2. (c) Three gland cells of Lmcg2 next to each other show that the gland cell seems to be dissolving. In the uppermost one the nuclei is already missing. (d) A Golgi (square) in the gland cell type Lmcg 1. (e) Underneath the cell layer muscles are recognizable. m = muscles, mi = microvilli, mo = mitochondria, n = nucleus, ve = vesicles.

Gland cell types

As the glowing mucus appears first at the pneumostome (Meyer-Rochow & Moore, 1988; pers. observations), one may speculate that the defence mucus, or at least its glowing component, is produced inside the mantle cavity. This is confirmed by earlier observations (Bowden, 1950; Greistorfer et al., 2023a), where the rest of the foot and its gland system were already investigated. Bowden (1950) stated that two big gland cell types present in this area are responsible for the glowing mucus, but this was refuted later (Greistorfer et al., 2023a; Meyer-Rochow & Moore, 1988). As the two big gland cell types (L11/L21) may be correlated with the defence mucus (Greistorfer et al., 2023a), they may produce the sticky mucus component, which gets mixed with the glowing component of different origin. The pneumostome lappet could be responsible for mixing and distributing the glowing mucus, even if the lappet is not actively moveable (Meyer-Rochow & Moore, 1988).

The mantle cavity and the gland cell types in this region show that there are two gland cell types in the roof of the mantle cavity (Lcmg1/Lcmg2) present over a large area. They are small, but present in high numbers. For the glowing of the defence mucus *Latia* luciferin, luciferase, oxygen and a so-called purple protein (Shimomura et al., 1966, 1972; Shimomura & Johnson, 1968a, 1968b) are required. It is definitely plausible that, for example, the purple protein is produced in Lmcg1 or Lmcg2 and later becomes combined with the sticky mucus from L11/L21 (Greistorfer et al., 2023a). Further, at least

the anterior part the mantle cavity is stuffed with mucus at the time of death of the animal. The release of the granular content of Lmcg1 into the mantle cavity is also detectable, and rough endoplasmic reticulum is present, which may be a sign of protein synthesis. In contrast, the gland type Lmcg2 seems to be holocrine, as different destruction stadiums can be seen. Further this gland cell type contains a large number of mitochondria and seemingly more Golgi than Lmcg1. This indicates high cellular activity and protein modification. This also supports the theory that some gland cell types in the mantle cavity are involved in the defence mucus production, although it remains unclear which ones. Then there is the question if the storage underneath the mentioned gland cell types in the mantle cavity has something to do with the defence mucus. This storage is lined with myosin filaments and this can lead to the conclusion that this area is contractile as well, but unfortunately no opening can be observed.

The histochemical staining reaction is another indication that at least Lmcg1 is involved in the production of defence mucus. Both, the vesicles as well as the released mucus in the mantle cavity, reacted identically to the PAS and Alcian blue stainings as the earlier tested released defence mucus (Greistorfer et al., 2023a). However, these stains are not very specific and numerous mucus producing glands react positively for sulphated and carboxylated glycoproteins (Greistorfer et al., 2020, 2023a; Grenon & Walker, 1978).

To get insight on the significance of the histochemical staining reactions, all prominent gland types in *L. neritoides* were investigated. Although the salivary gland, midgut gland and

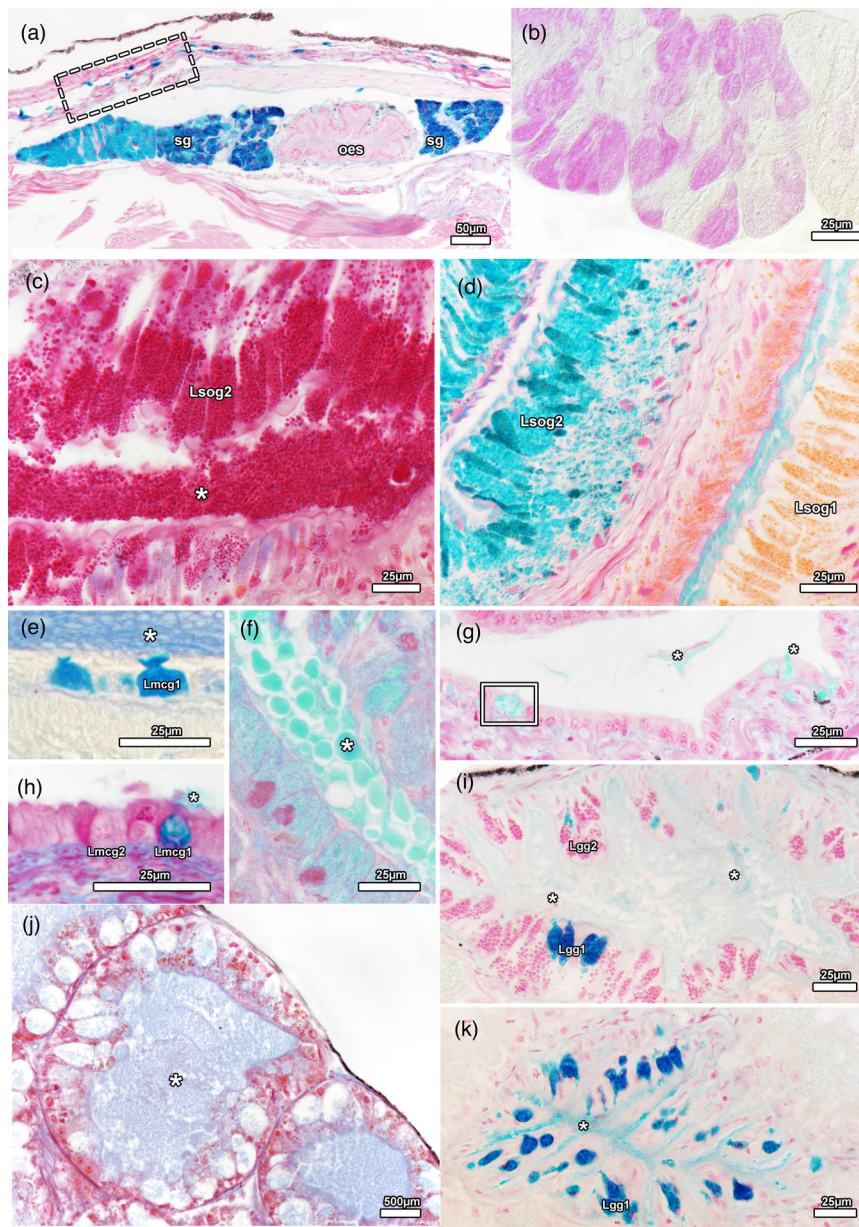


Figure 6 Histochemical staining of some gland types in *Latia neritoides*. (a) Overview of the oesophageal area. On both sides of the oesophagus the salivary gland shows a strong reaction to Alcian blue. Above the mantle cavity the gland type L1mcg (dashed square) is visible. (b) Close up of the cells of the salivary gland with some of them showing a reaction to PAS staining. (c) Azan staining. In the detailed view of the cells of Lsog2 the release of the coarse cell content is shown. (d) The difference between the staining reaction of Lsog1 and Lsog2 becomes visible. (e) The positive reaction to Alcian blue-PAS staining at pH 2.5 for the gland type Lmcg1 is shown. (f) The release of the granular content of the cells of albumen gland in distinct packages is visible. (g) The Lpag cells react positive to Alcian blue. (h) Lmcg1 and Lmcg2 shown next to each other. (i, k) Different regions of the intestinal loop show a different distribution pattern of Lgg1 and Lgg2. (j) Close up of a part of the midgut gland in an Azan staining. The secretion of the cells (asterisk) is nicely visible. (a, d, f–i, k) Azan and Alcian blue pH 1.0 combination staining. (c, e–k) Asterisks mark the released gland content. Lgg1 = *Latia* gut gland 1, Lgg2 = *Latia* gut gland 2, Lmcg1 = *Latia* mantle cavity gland 1, Lmcg2 = *Latia* mantle cavity gland 2, Lpag = *Latia* penis area gland, Lsog1 = *Latia* spermooviduct gland 1, Lsog2 = *Latia* spermooviduct gland 2, oes = oesophagus, sg = salivary gland.

albumen gland have already been noted in earlier works, their histochemical staining results have never been mentioned before (Eales, 1923; Meyer-Rochow & Moore, 1988;

Pelseneer, 1901). Our staining results of the salivary gland revealed two gland cell types. In addition, this study could show the regular appearance of Lgg1 and Lgg2 in different

Table 1 Histochemical analysis of some of *Latia neritoides*' gland types

Staining	Specificity	Lmcg1 (Latia mantle cavity gland 1)	Lmcg2 (Latia mantle cavity gland 2)	Salivary gland	Lgg1 (Latia gut gland 1)	Lgg2 (Latia gut gland 2)	Midgut gland	Albumen gland	Lsog1 (Latia spermoviduct gland 1)	Lsog2 (Latia spermoviduct gland 2)	Lpag (Latia penis area gland)
PAS	Carbohydrates	+	-	+ in some cells	+ -	-	+ - in a few cells	+	-	+ in some cells, which stained negative for BS	+
Alcian blue pH 1.0	Sulphated mucosubstances	+	-	++	++ in some cells	-	+ -	+ -	-	++	+
Alcian blue pH 2.5	Sulphated & carboxylated mucosubstances	+	-	++	++ in some cells	-	+ -	+ -	-	++	+
Alcian blue pH 1.0 + PAS	Sulphated glycoproteins	+	-	AB ++, PAS +	+	-	PAS + - in a few cells, AB + - in others	+	-	PAS + in some cells, AB + + in others	+
Alcian blue pH 2.5 + PAS	Sulphated & carboxylated glycoproteins	+	-	AB ++, PAS +	+	-	PAS + - in a few cells, AB + - in others	+	-	PAS + in some cells, AB + + in others	+
Toluidine blue pH 4.5	Acidic proteins	-	-	+ - didn't stain in all animals	+ - didn't stain in all animals	-	-	+ - didn't stain in all animals	-	++	-
Biebrich scarlet pH 6.0	Basic proteins	-	-	-	-	-	-	-	+	-	-
Biebrich scarlet pH 8.5		-	-	-	-	-	-	-	+	-	-
Biebrich scarlet pH 9.5		-	-	-	-	-	-	-	-	-	-
Biebrich scarlet pH 10.5		-	-	-	-	-	-	-	+ in some cells	-	-
von Kossa	Calcium	-	-	-	-	-	-	-	-	-	-
Alizarin Red S	Calcium	-	-	-	-	-	-	-	-	-	-
Arrow staining	L-DOPA	-	-	-	-	-	Not stained	Not stained	Not stained	Not stained	Not stained

++ = strong positive reaction, + = positive reaction, + - = weak reaction, - = no reaction. n.d., not differentiable; n.s., not stained; n.v., not visible.

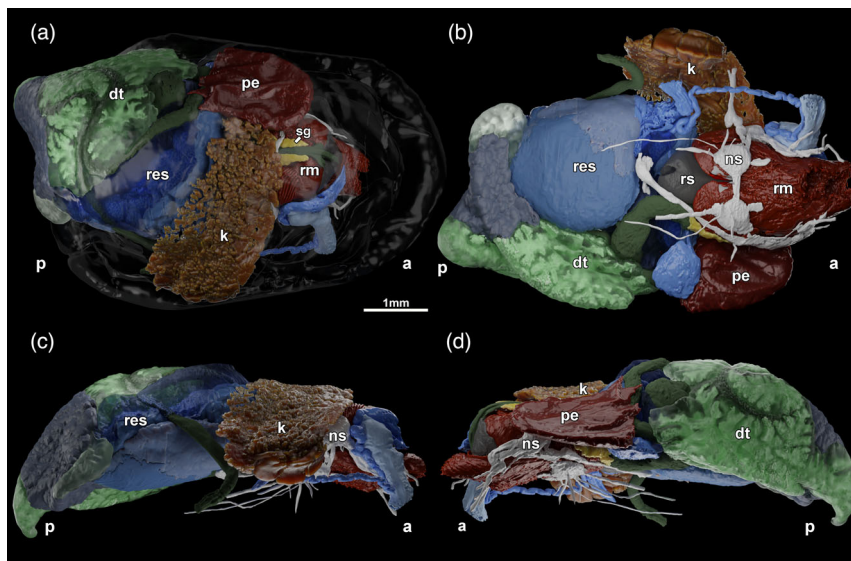


Figure 7 3D Visualization of *Latia neritoides* including all organ systems. (a) Dorsal view. Pericard and kidney overlap parts of the digestive tract, illustrated in green, and parts of the reproductive system, illustrated in blue. (b) Ventral view. The nervous system, mainly present in the anterior part of the animal, becomes visible. (c, d) Lateral views of the right (c) and left (d) sides. a = anterior, dt = digestive tract, k = kidney, ns = nervous system, p = posterior, pe = pericard, res = reproductive system, rm = radula musculature, rs = radula sack, sg = salivary gland.

gut sections as well as a distinct dissimilarity between Lsog1 and Lsog2 in the spermoviduct.

Morphology of the digestive tract

Our findings confirm previous studies (Eales, 1923; Meyer-Rochow & Moore, 1988; Pelseener, 1901) where the radula, its odontophores and its musculature are described as massive in proportion to the rest of the digestive system. The importance of the large muscle mass for scraping diatoms off rocks is also our interpretation. The salivary glands are described as elongated structures lying underneath the circum-oesophageal nerve ring (Eales, 1923) which could also be confirmed by the 3D model. The presence of a gizzard, a caecum and a single intestinal loop can be confirmed for *L. neritoides* (Eales, 1923; Meyer-Rochow & Moore, 1988; Pelseener, 1901). A very prominent digestive gland sits atop the other digestive tract components (Moore & Meyer-Rochow, 1988). The meaningful comparison of *L. neritoides* with other snails described in the older literature is difficult since the dissolution of Basommatophora as a taxon based on molecular phylogenetics and the changed relationships among families (Bouchet et al., 2017; Saadi et al., 2020). Nevertheless, in the family probably closest related to the Latidae, the Chiliniidae, *Chilina fluctosa* has a similarly organized digestive tract, although its gizzard is bi-lobed (Hubendick, 1978).

Morphology of the nervous system

Our data correlate largely with the initial description (Pelseener, 1901). The buccal ganglia are separated from each other, connected by a commissure (Eales, 1923). Our reconstruction

shows visceral and oesophageal ganglions situated closer to each other than previously described (Pelseener, 1901). Also, only one ganglion (supra-intestinal ganglion) is reported on the right side (Eales, 1923). We found this ganglion separated into two ganglia (parietal-/supraoesophageal ganglion), fitting the description of Pelseener (1901). In addition, our reconstructions show the left parietal ganglion situated next to the pleural ganglion, not as centred as described by Eales (1923).

In contrast to Hubendick (1945), who claimed the left parietal ganglion to be absent, we clearly confirm its presence, although on the left side it was admittedly less distinct than on the right side. This is in accordance to the latest study by Haszprunar and Huber (1990).

As mentioned above there are nerves projecting from the cerebral ganglia to the anterior part of the animal. Without any further specification, those nerves bifurcate into at least three (left) to four (right) nerves. Apparently, the anterior projections in *Limnea stagnalis* (Gastropoda, Lymnaeidae) also show such a separation into several distinct nerves (e.g. N. labialis minor/-opticus/-tacularis; Tuchina et al., 2012). In our study we couldn't follow the nerves to their termination points, as we did not use specific nerve stains. A similar situation as described by Tuchina et al. (2012) is assumed for *Latia*.

Morphology of the reproductive system

Generally, the reconstruction fits earlier investigations on the reproductive system of *L. neritoides* (Meyer-Rochow & Moore, 1988). It shows that the spermathecal duct discharges into the uterus and that the latter, the vagina and the vas deferens lead to the anterior region of the spermoviduct. The spermathecal duct joins at the very beginning at the end of the

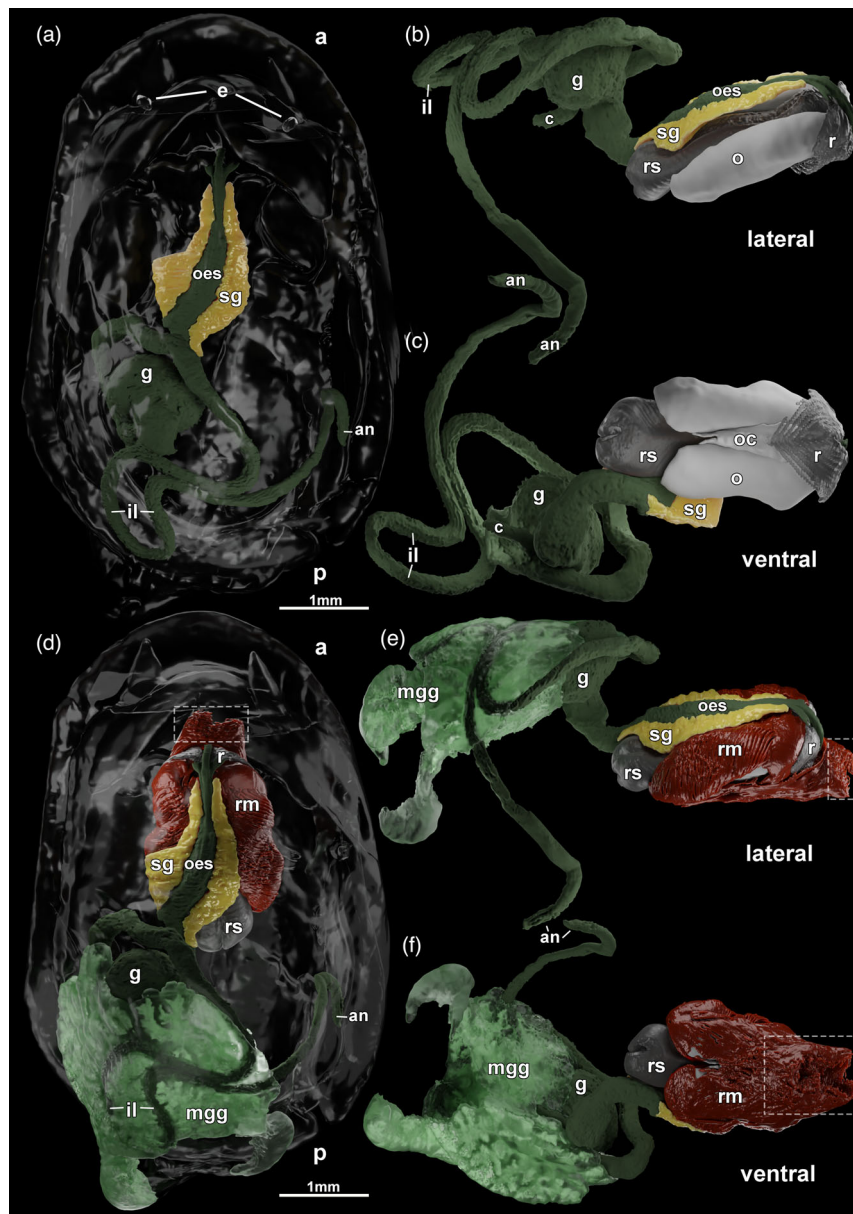


Figure 8 Reconstruction of the digestive tract of *Latia neritoides*. (a) Dorsal view of the digestive tract part, showing the location inside the animal. (b) Lateral view. The caecum is clearly visible, also the location of the radula and the odontophores next to the oesophagus. (c) Ventral view. The intestinal loop is shown, the caecum and the gizzard are visible. The ventral view of the odontophores reveals the connection between them. (d) The whole digestive system inside the body is reconstructed. (e, f) The midgut gland, overgrowing the intestine, is shown in light green. Inside its enormous branching is detectable. (d–f) A dashed square marks the area of the attachment of the radula musculature. a = anterior, an = anus, c = caecum, e = eye, g = gizzard, il = intestine loop, mgg = midgut gland, o = odontophores, oc = odontophores connection, oes = oesophagus, p = posterior, r = radula, rm = radula musculature, rs = radula sack, sg = salivary gland.

vagina, which is also described earlier (Meyer-Rochow & Moore, 1988). This is in contrast to the work of Eales (1923) in which the spermathecal duct leads to a more distant part of the vagina. The dissimilarity may be due to a different contraction status of the investigated animal. Further, the ovotestis, spermoviduct and albumen gland are all of a similar and relatively big size (Meyer-Rochow & Moore, 1988; Moore & Meyer-Rochow, 1988). Like previous authors (Eales, 1923;

Meyer-Rochow & Moore, 1988), we were unable to identify the prostate gland mentioned by Pelseneer (1901).

Morphology of the heart and kidney

We found the same results as presented in Pelseneer (1901): a heart with a closed pericardium situated on the left side of the body. A single kidney sits on the right side of the body.

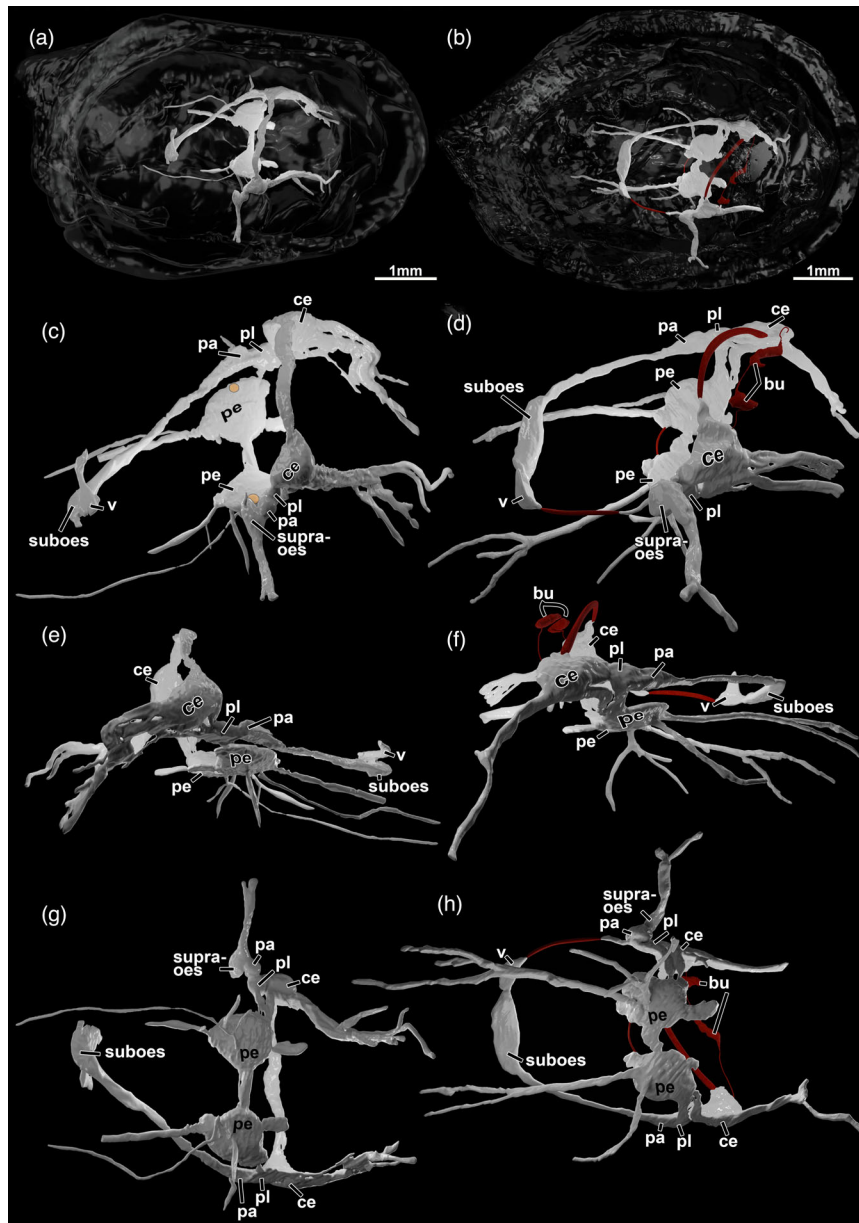


Figure 9 Reconstruction of the nervous system of *Latia neritoides* based on μ -CT (a, c, e and g) and HREM data (b, d, f and h). (a, b) Dorsal view. (c) The location of the statocysts are marked in yellow. (c, d) Dorsolateral view of the right side. (e, f) Lateral view of the left side. (g, h) Ventral view. (b, d, f, h) In red the nervous system is complemented with the reconstruction based on serial sections of a third animal. bu = buccal ganglion, ce = cerebral ganglion, pa = parietal ganglion, pe = pedal ganglion, pl = pleural ganglion, suboes = suboesophageal ganglion, supraoes = supraoesophageal ganglion, v = visceral ganglion.

Conclusion and outlook

We conclude that the first ever 3D model of *Latia neritoides* makes it definitely easier to understand the anatomical positions of the various organ systems relative to each other and their locations inside the animal. In general, this 3D model could also substantiate previous investigations. Our investigation on the mantle cavity at the ultrastructural level is beyond

doubt of considerable importance for bioluminescence and physiological research in *L. neritoides*.

Although the study could not completely solve the mystery of the origin of the production of the glowing mucus, it brings new insights into this topic and a first description of the gland types present in the mantle cavity. Further investigations at proteomic and transcriptomic level are likely to

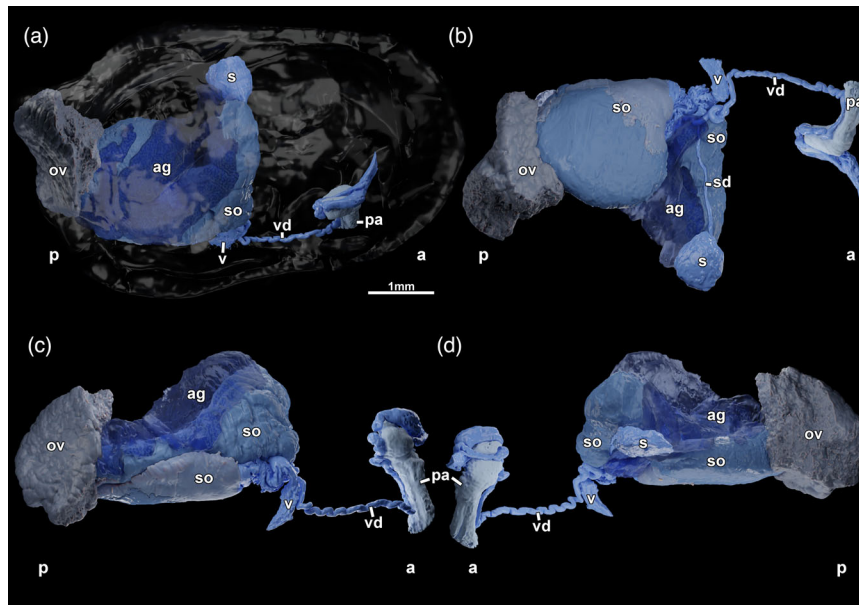


Figure 10 Reconstruction of the reproductive system of *Latia neritoides*. (a) Dorsal view. (b) Ventral view. (c, d) Lateral view. (c) View of the right side. (d) View of the left side. a = anterior, ag = albumen gland, ov = ovotestis, p = posterior, pa = penile apparatus, s = spermatheca, sd = spermathecal duct, so = spermooviduct, v = vagina, vd = vas deferens.

lead to a deeper understanding of this issue and the actual composition and functionality of the mucus.

Funding information

Sophie Greistorfer was recipient of a DOC Fellowship of the Austrian Academy of Sciences (DOC [Doctoral Fellowship Programme of the Austrian Academy of Sciences]/25023) at the Unit for Integrative Zoology, Department of Evolutionary Biology, University of Vienna, Austria and got the 6 month VDSSEE (Vienna Doctoral School for Ecology and Evolution) completion grant. The sampling field trip was additionally supported by the Austrian Science Fund FWF (Project P31612-21).

Author contributions

GS and SG planned and designed the study. GS and IM supervised the study. JvB, SG and VBM-R collected field data. SGe and WW generated some data. SG generated and interpreted the data. SG wrote the first draft, GS, IM, JvB, VBM-R, SGe and WW revised the manuscript. All authors read and approved of the final manuscript at submission.

Acknowledgments

We want to thank the Department of Evolutionary Biology, Unit Integrative Zoology, University of Vienna, Austria, for making the resources available. Further we like to thank Julian Bibermaier, MSc and Johannes Suppan, MSc for providing the TEM sections and Kevin Pfeifer, PhD (Archaea Biology and Ecogenomics

Unit) for providing and enable the use uranyl acetate to contrast them. Eventually, we thank the Core Facility Cell Imaging and Ultrastructure Research (University of Vienna, Austria) for the possibility to obtain electron scanning images during the course ‘Spezielle Techniken in der Elektronenmikroskopie und Ultrastrukturforschung (2021)’. In addition, our thanks are going to Brian Smith (Freshwater Ecologist, NIWA, Hamilton, New Zealand) for the cooperation with field work in New Zealand and Dr Thomas Schwaha for establishing contacts between research facilities. Further we want to thank Dr Andy Sombke and Brain Metscher, Privatdoz. PhD for providing the μ -CT stack, Phil Novis, from Landcare Research, New Zealand, for the help with the identification of the diatoms and Ao. Univ.-Prof. i. R. Dr Waltraud Klepal for help with the evaluation of some TEM images. VBM-R wishes to thank President Dr James Jin-Kyung Kim and Dean Doing Hoon Ko of PUST for their support during his stay at Pyongyang University of Science and Technology and discussions on gastropod physiology including *Latia neritoides*.

References

- Aescht, E., Büchl-Zimmermann, S., Burmester, A., Stefan, D.-P., Desel, C., Hamers, C., Jach, G., Kässens, M., Makovitzky, J., Mulisch, M., Nixdorf-Bergweiler, B., Pütz, D., Riedelsheimer, B., van den Boom, F., Wegerhoff, R., & Welsch, U. (2010). *Romeis Mikroskopische Technik* (18th ed.). Spektrum Akademischer Verlag.
- Arnou, L. E. (1937). Colorimetric determination of the components of 3,4-dihydroxyphenylalanine-tyrosine mixtures. *The Journal of Biological Chemistry*, **118**, 531–537.

- Bouchet, P., Rocroi, J. P., Hausdorf, B., Kaim, A., Kano, Y., Nützel, A., Parkhaev, P., Schrödl, M., & Strong, E. E. (2017). Revised classification, nomenclator and typification of gastropod and monoplacophoran families. *Malacologia*, **61**, 1–526.
- Bowden, B. J. (1950). Some observations on a luminescent freshwater limpet from New Zealand. *The Biological Bulletin*, **99**, 373–380.
- Counsilman, J. J., Loh, D., Chan, S. Y., Tan, W. H., & Copeland, J. (1987). Factors affecting the rate of flashing and loss of luminescence in a Asian land snail, *Dyakia striata*. *Veliger*, **29**, 394–399.
- Counsilman, J. J., & Ong, P. P. (1988). Responses of the luminescent land snail *Dyakia (Quantula) striata* to natural and artificial lights. *Journal of Ethology*, **6**, 1–8.
- Deheyn, D. D., & Wilson, N. G. (2011). Bioluminescent signals spatially amplified by wavelength-specific diffusion through the shell of a marine snail. *Proceedings of the Royal Society B: Biological Sciences*, **278**, 2112–2121.
- Eales, N. B. (1923). Mollusca. In British Museum (Natural History) (Ed.), *British Antarctic (“Terra Nova”) expedition, 1910: Natural history reports zoology* (pp. 1–45). British Museum.
- Geyer, S. H., Maurer-Gesek, B., Reissig, L. F., & Weninger, W. J. (2017). High-resolution episcopic microscopy (HREM) – simple and robust protocols for processing and visualizing organic materials. *Journal of Visualized Experiments*, **125**, 1–11. <https://doi.org/10.3791/56071>
- Gould, J., Valdez, J. W., & Upton, R. (2019). Adhesive defence mucus secretions in the red triangle slug (*Triboniophorus graeffei*) can incapacitate adult frogs. *Ethology*, **125**, 587–591.
- Greistorfer, S., Suppan, J., Cyran, N., Klepal, W., Farkas, R., Rudoll, L., & von Byern, J. (2020). Characterization of the *Arion vulgaris* pedal gland system. *Journal of Morphology*, **281**, 1059–1071.
- Greistorfer, S., von Byern, J., Miller, I., Meyer-Rochow, V. B., Farkas, R., & Steiner, G. (2023a). A histochemical and morphological study of the mucus producing pedal gland system in *Latia neritoides* (Mollusca; Gastropoda; Hygrophila). *Zoology*, **156**, 126067.
- Greistorfer, S., von Byern, J., Miller, I., Meyer-Rochow, V. B., Farkas, R., & Steiner, G. (2023b). Corrigendum to “A histochemical and morphological study of the mucus producing pedal gland system in *Latia neritoides* (Mollusca; Gastropoda; Hygrophila)” [zoology 156 (2023a)]. *Zoology*, **159**, 126101.
- Grenon, J. F., & Walker, G. (1978). The histology and histochemistry of the pedal glandular system of two limpets, *Patella vulgata* and *Acamea tessulata* (gastropoda: Prosobranchia). *Journal of the Marine Biological Association of the United Kingdom*, **58**, 803–816.
- Grey, J. E. (1850). Description of a new genus and several new species of terrestrial, fluviatile, and marine molluscous animals inhabiting New Zealand. *Proceedings of the Zoological Society of London*, **17**, 164–169.
- Haddock, S. H., Moline, M. A., & Case, J. F. (2010). Bioluminescence in the sea. *Annual Review of Marine Science*, **2**, 443–493.
- Haszprunar, G., & Huber, G. (1990). On the central nervous system of Smeagolidae and Rhodopidae, two families questionably allied with the Gymnomorpha (Gastropoda: Euthyneura). *Journal of Zoology*, **220**, 185–199.
- Heidenhain, M. (1905). Über die Anwendung des Azokarmins und der Chromotrope. *Zeitschrift für Wissenschaftliche Mikroskopie und für Mikroskopische Technik*, **XXII**, 337–343.
- Hubendick, B. (1945). *Phylogenies und Tiergeographie der Siphonariidae. Zur Kenntnis der Phylogenie in der Ordnung der Basomatophora und des Ursprungs der Pulmonatengruppe*. Dissertation, Zoologiska Bidrag från Uppsala.
- Hubendick, B. (1978). Systematics and comparative morphology of the Basomatophora. In V. Fretter & J. Peake (Eds.), *Pulmonates. Volume 2A. Systematics, evolution, and ecology* (pp. 1–84). Academic Press.
- Hutton, F. W. (1881). Notes on some Pulmonate Mollusca. *Transactions and Proceedings of the Royal Society of New Zealand*, **14**, 156.
- Kelly, P. M., & Cory, J. S. (1987). Operculum closing as a defence against predatory leeches in four British freshwater prosobranch snails. *Hydrobiologia*, **144**, 121–124.
- Kilroy, C. (2020). Quick guide to common diatom genera in freshwaters. In G. Cristobal, S. Blanco, & S. Bueno (Eds.), *Development in applied phycology 10: Modern trends in diatom identification* (pp. 33–37). Springer Nature Switzerland AG.
- Lösel, P. D., van de Kamp, T., Jayme, A., Ershov, A., Faragó, T., Pichler, O., Tan Jerome, N., Aadepe, N., Bremer, S., Chilingaryan, S. A., Heethoff, M., Kopmann, A., Odar, J., Schmelzle, S., Zuber, M., Wittbrodt, J., Baumbach, T., & Heuveline, V. (2020). Introducing Biomedisa as an open-source online platform for biomedical image segmentation. *Nature Communications*, **11**, 5577.
- Mair, J., & Port, G. (2002). The influence of mucus production by the slug, *Deroceras reticulatum*, on predation by *Pterostichus madidus* and *Nebria brevicollis* (Coleoptera: Carabidae). *Biocontrol Science and Technology*, **12**, 325–335.
- Marshall, B. A. (1997). A luminescent euimid (Mollusca: Gastropoda) from New Zealand. *Molluscan Research*, **18**, 69–72.
- Martin, A. W., & Deyrup-Olsen, I. (1986). Function of the epithelial channel cells of the body wall of a terrestrial slug, *Ariolimax columbianus*. *Journal of Experimental Biology*, **121**, 301–314.
- McManus, J. F. A., & Mowry, R. W. (1960). *Staining methods: Histological and histochemical*. Paul Hoeber Inc.
- Metscher, B. (2022). Fiji (ImageJ) plugin to read Xradia XRM files. Zenodo. <https://doi.org/10.5281/zenodo.7124263>
- Meyer-Rochow, V. B., & Bobkova, M. V. (2001). Anatomical and ultrastructural comparison of the eyes of two species of aquatic, pulmonate gastropods: The bioluminescent *Latia*

- neritoides* and the non-luminescent *Ancylus fluviatilis*. *New Zealand Journal of Marine and Freshwater Research*, **35**, 739–750.
- Meyer-Rochow, V. B., & Moore, S. (1988). Biology of *Latia neritoides* GRAY 1850 (Gastropoda, Pulmonata, Basomatophora): The only light-producing freshwater snail in the world. *Internationale Revue der Gesamten Hydrobiologie und Hydrographie*, **73**, 21–42.
- Meyer-Rochow, V. B., & Moore, S. (2009). Hitherto unreported aspects of the ecology and anatomy of a unique gastropod: The bioluminescent freshwater pulmonate *Latia neritoides*. In V. B. Meyer-Rochow (Ed.), *Bioluminescence in focus – a collection of illuminating essays* (pp. 85–104). Research Signpost.
- Mohun, T. J., & Weninger, W. J. (2012a). Episcopic three-dimensional imaging of embryos. *Cold Spring Harbor Protocols*, **6**, 641–646. <https://doi.org/10.1101/pdb.top069567>
- Mohun, T. J., & Weninger, W. J. (2012b). Embedding embryos for high-resolution episcopic microscopy (HREM). *Cold Spring Harbor Protocols*, **6**, 678–680. <https://doi.org/10.1101/pdb.prot069583>
- Moore, S., & Meyer-Rochow, V. B. (1988). Observations on habitat and reproduction in the pulmonate, basomatophoran gastropod *Latia neritoides* GRAY 1850 – the only bioluminescent freshwater mollusc in the world. *Verhandlungen des Internationalen Verein Limnologie*, **23**, 2189–2192.
- Morii, Y., Prozorova, L., & Chiba, S. (2016). Parallel evolution of passive and active defence in land snails. *Scientific Reports*, **6**, 35600.
- Mulisch, M., & Welsch, U. (2010). *Romeis Mikroskopische Technik* (18th ed.). SpringerSpektrum.
- Oba, Y., & Schultz, D. T. (2014). Eco-evo bioluminescence on land and in the sea. In G. Thouand & R. Marks (Eds.), *Bioluminescence fundamentals and applications in biotechnology* (pp. 3–36). Springer-Verlag Berlin Heidelberg.
- Ohmiya, Y., Kojima, S., Nakamura, M., & Niwa, H. (2005). Bioluminescence in the limpet-like snail, *Latia neritoides*. *Bulletin of the Chemical Society of Japan*, **78**, 1197–1205.
- Ovando, X. M. C., & Gregoric, D. E. G. (2012). Systematic revision of *Chilina gray* (Gastropoda: Pulmonata) from northwestern Argentina and description of a new species. *Malacologia*, **55**, 117–134.
- Pelseneer, P. (1901). *Études sur des gastropodes pulmonés*. Mémoires de l'Académie royale des sciences, des lettres et des beaux-arts de Belgique.
- Ponder, W. F. (1964). The freshwater Mollusca of New Zealand. *Tane*, **10**, 12–35.
- Ponder, W. F. (1988). Bioluminescence in *Hinea braziliana* (Lamarck) (gastropoda: Planaxidae). *Journal of Molluscan Studies*, **54**, 361.
- Ruyter, J. H. C. (1931). Eine einfache Methode für das Aufkleben von Zelloidin-Paraffinschnitten. *Zeitschrift für Wissenschaftliche Mikroskopie und für Mikroskopische Technik*, **48**, 226–227.
- Saadi, A. J., Davison, A., & Wade, C. M. (2020). Molecular phylogeny of freshwater snails and limpets (Panpulmonata: Hygrophila). *Zoological Journal of the Linnean Society*, **190**, 518–531.
- Sheehan, D., & Hrapchack, B. (1980). *Theory and practice of histotechnology* (2nd ed.). Mosby.
- Shimomura, O., & Johnson, F. H. (1968a). Purification and properties of the luciferase and of a protein cofactor in the bioluminescence system of *Latia neritoides*. *Biochemistry*, **7**, 2574–2580.
- Shimomura, O., & Johnson, F. H. (1968b). The structure of *Latia luciferin*. *Biochemistry*, **7**, 1734–1738.
- Shimomura, O., Johnson, F. H., & Haneda, Y. (1966). Isolation of the luciferin of the New Zealand fresh-water limpet, *Latia neritoides* gray*. In F. H. Johnson & Y. Haneda (Eds.), *Bioluminescence in Progress* (pp. 391–404). Princeton University Press.
- Shimomura, O., Johnson, F. H., & Kohama, Y. (1972). Reactions involved in bioluminescence systems of Limpet (*Latia neritoides*) and luminous bacteria. *Proceedings of the National Academy of Sciences of the United States of America*, **69**, 2086–2089.
- Smith, A. M. (2006). The biochemistry and mechanics of gastropod adhesive gels. In A. M. Smith & J. A. Callow (Eds.), *Biological adhesives* (pp. 167–182). Springer-Verlag.
- Spicer, S. S., & Lillie, R. D. (1961). Histochemical identification of basic proteins with Biebrich scarlet at alkaline pH. *Stain Technology*, **6**, 365–370.
- Suter, H. (1913). *Manual of the New Zealand Mollusca. With and atlas of quarto plates*. Government Printer.
- Tuchina, O. P., Zhukov, V. V., & Meyer-Rochow, V. B. (2012). Central and peripheral neuronal pathways revealed by backfilling with neurobiotin in the optic, tentacular and small labial nerves of *Lymnaea stagnalis*. *Acta Zoologica*, **93**, 28–47.
- Widder, E. (2010). Bioluminescence in the ocean: Origins of biological, chemical, and ecological diversity. *Science*, **328**, 704–708.

Supporting Information

Additional Supporting Information may be found in the online version of this article:

Video S1. Characterization of the gland cell types present in the mantle cavity of *Latia neritoides*. The animation displays the reconstructed mantle cavity and the gland cell types present there. A morphological as well histochemical characterization is demonstrated.

Video S2. Morphological analyses of *Latia neritoides* and some of its gland cell types. The animation shows the bauplan and the location of gland cell types. Also a histochemical characterization of this gland cell types is shown.